Theory and Design of the Surface Acoustic Wave Multistrip Coupler

F. GRAHAM MARSHALL, CLELAND O. NEWTON, AND EDWARD G. S. PAIGE

Invited Paper

***Abstract*—The multistrip coupler performs the function of a directional coupler for freely propagating surface acoustic waves on a piezoelectrically active substrate. Its operation is analyzed in terms of a transmission line based equivalent circuit. Expressions are obtained for the directionality (transmission and reflection) in terms of the number of coupler strips and the acoustic frequency. Theory and experiment are shown to be in very good agreement. 50-percent metallization is found to give optimum performance; progressive increase in the proportion of the coupler area covered with metal is shown to involve a progressive change from an in-line field model to a crossed-field model.**

Outside a stopband region it is found that a simplified expression for the directionality is valid; this greatly facilitates component design. Design criteria for multistrip components are discussed in terms of substrate and bandwidth requirements. An analysis is included of resistive and capacitative effects on coupling, and problems associated with coupling between dissimilar materials are discussed.

I. Nomenclature

A	Upper track as defined in Fig. 1.
(a)	Antisymmetric mode.
B	Lower track (Fig. 1).
C	Capacitance between adjacent strips for individual track aperture.
$C1$–$C9$	Multistrip couplers as listed in Table I.
d	Repeat distance of periodic multistrip coupler.
F	Geometric filling factor.
F_T	Fraction of energy transferred between tracks.
f	Surface-acoustic-wave frequency.
f_n	Normalized frequency $(=f/f_0)$
f_0	Frequency of fundamental structure stopband $(=v/2d)$.
i	Equivalent circuit current.
K^2	Electromechanical coupling constant.
L_T	Coupler length for complete energy transfer between tracks.
l	Aperture width of individual track.
MSC	Multistrip coupler.
N	Number of strips.
N_T	Number of strips for complete energy transfer between tracks.
P	Power in individual track.
R_F	Resistance of strip along an individual track aperture.
r	Transformer turns ratio in equivalent circuit.
SAW	Surface acoustic wave.
(s)	Symmetric mode.
v	Surface-acoustic-wave velocity.
v_a	Antisymmetric mode velocity.
v_s	Symmetric mode velocity.
Z	Impedance of individual track.
α	Active fraction of periodic repeat distance of MSC.
α_R	Energy attenuation coefficient for antisymmetric wave.
γ	Parameter for proportion of crossed to in-line field model.
Δl	Separation distance between coupled tracks.
Δv	Difference between free and metallized propagation velocities.
η	Metallization ratio; strip width equals ηd.
θ	Phase elapse angle for transmission line.
λ	SAW wavelength.
μ	Mismatch coefficient for impedances.
ρA	Mass per unit track length.
ϕ	Phase elapse angle perturbed from θ by coupling action.

Manuscript received October 4, 1972; revised October 23, 1972.

The authors are with the Royal Radar Establishment, Great Malvern, Worcestershire, England.

II. Introduction

A. The Basic Component

THE multistrip coupler (MSC) [1] is a directional coupler for use with surface acoustic waves. It consists of an array of parallel metallic strips on a piezoelectric substrate. Its specific property is the coupling of nonguided acoustic waves on a single substrate in contrast to the operation of both the waveguide coupler [2] and the adjacent medium coupler [3].

The periodic MSC is shown schematically in Fig. 1. If a surface acoustic wave is launched from one of the transducers into one half of the structure [track A, for example, Fig. 1(a)], potential differences are set up between adjacent metal strips because the substrate is piezoelectric. These potentials also appear in track B where a second surface acoustic wave is generated.

In common with other simple coupled mode systems, the behavior of the coupler is best described in terms of the modes of the system, a mode being a field pattern which is not distorted during propagation. In the elementary case of parallel equal aperture tracks on a uniform piezoelectric medium, the modes can be identified(Section III-A2) as the symmetric mode s and the antisymmetric mode a as shown in Fig. 1(b). Any input pattern that is uniform in the individual tracks can be decomposed into these two modes. In general, the symmetric and antisymmetric modes will propagate with different velocities, v_s and v_a, respectively. It is the beating of these two modes which leads to a periodic change of energy between tracks and hence to the coupling action.

In design, manufacture, and use the MSC is compatible with the conventional interdigital transducer. No extra processing stages are involved in the photolithographic

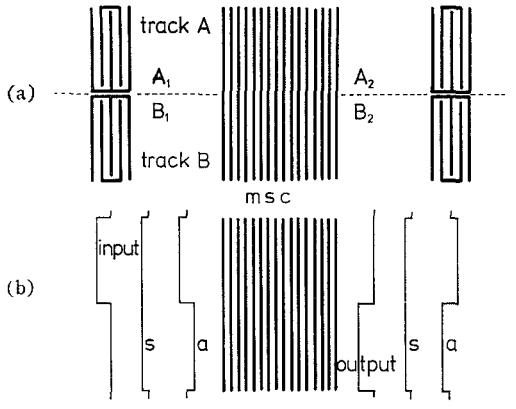

Fig. 1. (a) Schematic of multistrip directional coupler with interdigital transducers at input and output ports. (b) Input and output field distributions resolved into symmetric s and antisymmetric a modes for a coupler in which 100-percent transfer from track A to track B occurs.

reproduction; the precision required is similar to that for the interdigital transducers used to drive the system. No connections, internal or external, are required by the coupler. Thus no penalty is paid by the introduction of the coupler other than the occupation of space on the substrate and the additional delay time necessary for the wave to traverse the structure. On material of high electromechanical coupling constant, such as lithium niobate, the penalty is not severe.

A family of surface-wave components has been derived from the MSC in addition to its use as a conventional directional coupler. The family includes broad-band highly reflecting mirrors, broad-band unidirectional transducers, broad-band triple transit suppressors, beamwidth changers (SAW impedance transformers), and redirectors of acoustic beams. These components are listed and described in [17]. The objective of this paper is to present a theory of the periodic MSC based on an equivalent circuit model and hence to established design criteria which are relevant both to the coupler and to components derived from it.

B. Approach to the Analysis

Our primary concern in this paper is to develop usable design criteria for the MSC—criteria which employ reasonably simple analytical expressions. This is one of the main reasons for adopting an electrical equivalent circuit model from the outset. The model which we use to fit the experimental data (Section IV) is no more sophisticated than that used previously to account for the behavior of interdigital surface-wave transducers [5]. Furthermore, the parameters required to fit a wide range of gap to strip width ratios for the MSC on lithium niobate show a striking resemblance to those employed for interdigital transducers [4] on a poled PZT ceramic [5].

The main frequency range of interest for prediction of MSC performance lies in a broad band below the frequency of the first stopband. This stopband is a specific feature of periodic couplers and occurs at the main structure resonance frequency $f_0=v/2d$, where v is the surface-wave velocity and d is the MSC periodic repeat distance. In this frequency range, simple analytical expressions are found which predict performance very satisfactorily; these are used extensively in [17] when analyzing device performance. Another virtue of the equivalent circuit approach is that factors such as resistivity of metal strips and added capacitance can be readily incorporated (Section V).

C. Essence of MSC Behavior

It is useful as a preliminary stage to demonstrate the behavior of the coupler simply in terms of the electromechanical coupling constant K^2. The model of the MSC employed in this instance is that of the perfectly anisotropic film of Marshall and Paige [1]. The film spans a pair of surface acoustic tracks. Its conductivity parallel to the surface-wave vector is zero; its conductivity perpendicular to the wave vector is infinite. The velocity of the symmetric mode v_s is the stiffened velocity, since no current can flow parallel to the propagation direction; but since current can flow perpendicular to this direction, charges in the two tracks associated with the antisymmetric mode will cancel each other out and the velocity of this mode v_a is the unstiffened velocity. The length for 100-percent transfer of energy, referred to as the transfer length L_T, is obtained in terms of the acoustic wave frequency f as half the beat wavelength for the modes. Thus,

$$L_T = \frac{1}{2f}\frac{v_s v_a}{v_s - v_a} = \frac{\lambda}{K^2} \tag{1}$$

where λ is the surface acoustic wavelength and K^2 is given by [6] as

$$K^2 = 2\frac{\Delta v}{v}. \tag{2}$$

The number of metal strips involved is obtained as

$$N_T = \frac{\lambda}{K^2 d} \tag{3}$$

assuming total activity. This demonstrates the close relationship between the size of the coupler and the value of K^2.

In practice, however, the periodic MSC differs from the perfectly anisotropic film in two main ways: 1) stopbands are introduced by the periodicity; 2) coupling efficiency is reduced by geometric factors which depend on the metallization.

To gain an insight into the significance of the second factor, consider a sinusoidal signal sampled in one track and regenerated in the second track by a periodic structure (the MSC). The sampling frequency is significant if only a few samples are taken per wavelength. The sampling element width is significant if it is comparable to a wavelength because only the instantaneous average of signal amplitude across the sampling window can be transmitted to the second track. If the phase shift in the sampling window is θ, the coupled intensity is reduced by the factor

$$\left(\frac{\sin(\theta/2)}{\theta/2}\right)^2. \tag{4}$$

θ is given by $2\pi\alpha d/\lambda$ where αd is the active length in each repeat distance. Incorporation of the reduced effectiveness due to sampling and of the effective repeat distance gives

$$N_T = \frac{\lambda}{K^2 \alpha d}\left(\frac{\sin(\theta/2)}{\theta/2}\right)^{-2}. \tag{5}$$

This expression is very similar to that which results from

simplifying the detailed equivalent circuit approach developed in Section III. It illustrates how coupler action works but does not demonstrate a stopband.

An alternative approach is to consider a pair of strips to be equivalent to a single finger pair transducer located in each track, one feeding the other directly through their electrical ports. This is the approach taken up in Section III. It illustrates the broad bandwidth inherent in the MSC structure in that no strips are interconnected. Very good agreement between prediction and experiment is obtained, using empirical parameters.

The ultimate approach involves a self-consistent computation of the piezoelectric properties of the particular material to yield exact electric field configurations and hence all coupling parameters [4], [7], [8]. This is outside the scope of a paper on design criteria in view of the success of the equivalent circuit approach.

III. Equivalent Circuit Theory of the MSC

A. The Equivalent Circuit Model

1) Transducer Assembly: The MSC, spanning a pair of acoustic tracks, may be viewed as a structure whose repeat distance can be represented by a transducer in one track connected to a transducer in the other track through their electrical ports; this concept was presented in the introduction. Thus the coupler as a whole can be represented as an assembly of interconnected transducers. Smith *et al.* [9] in their analysis of interdigital surface-wave transducers used equivalent circuit models based on those employed for bulk wave transducers. In view of the success of their analysis we shall adopt the same bulk wave transducer circuit models. These are the so-called in-line and crossed-field models. The in-line model is employed when the electrical field vector and the wave vector are collinear; it pertains primarily to gaps between electrodes. The crossed-field model is employed when electric field and wave vector are perpendicular; it pertains primarily to regions under electrodes. Two elaborations of the equivalent circuit of Smith *et al.* [9] are employed. Following Kraiojananan and Redwood [10] we introduce a passive transmission line element into each section, and following Milsom and Redwood [5] we employ mixed models which can be intermediate between in-line and crossed field.

Fig. 2 illustrates the equivalent circuit model applied to each MSC repeat distance, termed a section. Identical acoustic tracks have been assumed for simplicity. Each track is regarded as a transmission line and is represented by T networks. Each section comprises a passive element (subscript 1) and an active element (subscript 2) of impedance Z_i, propagation velocity v_i, and unperturbed phase shift θ_i. The active fraction α of the section is introduced by writing

$$\theta_1 = \frac{2\pi f(1-\alpha)d}{v_1} \qquad \theta_2 = \frac{2\pi f\alpha d}{v_2}. \tag{6}$$

The ratio of wave velocities in the elements is defined by a parameter μ, where

$$v_2/v_1 = (1 - \tfrac{1}{2}\mu K^2). \tag{7}$$

Thus μ takes the significance of a loading term related to the piezoelectric stiffening. We consider

$$Z_i = \rho A v_i \tag{8}$$

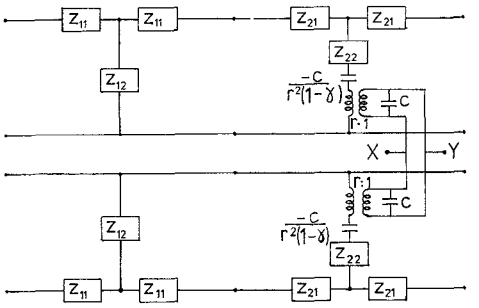

Fig. 2. Transmission line equivalent circuit for one repeat distance of MSC showing a pair of coupled lines with passive and active elements.

where ρA is the substrate mass per unit track length. Then the element impedance values for Fig. 2 are given [9] by

$$Z_{i1} = jZ_i \tan(\theta_i/2) \tag{9a}$$

$$Z_{i2} = -jZ_i \operatorname{cosec} \theta_1. \tag{9b}$$

The value of γ associated with the negative capacitor of the active element in Fig. 2 determines whether an in-line model ($\gamma = 0$) or a crossed-field model ($\gamma = 1$) has been adopted; it permits the additional flexibility that a mixed model ($0 < \gamma < 1$) can be investigated [5]. The electrical ports, represented by the secondary circuits of idealized transformers of turns ratio $r{:}1$, are connected from one line to the other to give coupling action. The transformer turns ratio is obtained, as for surface-wave transducers, from the bulk wave result of Berlincourt *et al.* [11] as

$$r^2 = FK^2 \frac{v_2}{\alpha d} Z_2 C. \tag{10}$$

Here F is a filling, or geometric, factor which depends on the degree of mentallization. The preceding result is obtained for both in-line and crossed-field models and is taken to apply to mixed models also.

2) Normal Modes: We consider normal modes of the coupler at this stage because with their aid an important simplification can be made in the equivalent circuit: the two coupled transmission lines can be analyzed in terms of wave propagation on a single line.

The modes of the coupler, symmetric and antisymmetric, have been discussed in the Introduction and illustrated in Fig. 1(b). The modes are now defined by reference to coupled potential (electrical potential on each strip) and coupled flux (charge flowing from one line to the other). The symmetric mode is defined as the condition of zero coupled flux. It is essentially a wave launched with the same amplitude and phase in each track. Because the velocity is the same in each track, phase and amplitude correspondence is maintained during propagation irrespective of whether or not the metal strips are connected at the line separating the two tracks. The potentials on corresponding strips in each track are identical whether joined or not; consequently, no charge flows between them giving the condition of zero coupled flux. The antisymmetric mode is defined as the condition of zero coupled potential. The mode is composed of waves propagating in the two tracks in antiphase; equal and opposite surface charges would be generated in each strip if they were not joined. By connecting them charge flows and exact compensation takes

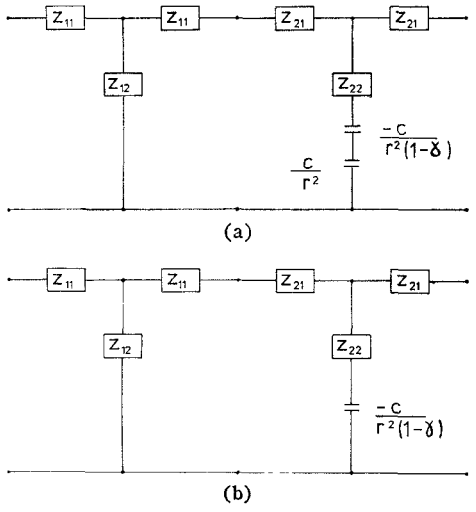

Fig. 3. Single-line equivalent circuits. (a) For symmetric mode. (b) For antisymmetric mode. $\gamma=0$ gives the in-line model, $\gamma=1$ the crossed-field model, and $0<\gamma<1$ the mixed model.

place. Consequently, no potential appears at any element and the condition of zero coupled potential applies.

Exactly the same argument can be applied to the system of Fig. 2, with the substitution of "transmission line" for "acoustic track." This establishes a correspondence between coupler and equivalent circuit.

3) Reduction of Equivalent Circuit to a Single Transmission Line: Since for the symmetric mode the waves on the two lines propagate without interaction, propagation is unaffected if the equivalent circuit is open circuit at X and Y; the system can be represented by a single line with an open circuit across the capacitance C of Fig. 2 (at XY) in every section. For the antisymmetric mode, the waves propagate so that each element is at zero potential. This is equivalent to a single line with a short circuit across the capacitance C (at XY) in every section. The resulting single-line equivalent circuits are shown in Fig. 3 for either mode. In effect, Z_{22} has become

$$Z_{22}(s) = -j\left(Z_2 \operatorname{cosec}(\theta_2) + \frac{\gamma r^2}{\omega C}\right) \tag{11a}$$

$$Z_{22}(a) = -j\left(Z_2 \operatorname{cosec}(\theta_2) - \frac{(1-\gamma)r^2}{\omega C}\right) \tag{11b}$$

representing symmetric mode (s) and antisymmetric mode (a).

4) Deduction of Coupler Behavior: The phase shifts across each section for the symmetric and antisymmetric modes are given by

$$\phi(s) = \cos^{-1}\left(\frac{Z_T^2(s) - Z_{12}^2 - Z_{22}^2(s)}{2Z_{12}Z_{22}(s)}\right) \tag{12a}$$

$$\phi(a) = \cos^{-1}\left(\frac{Z_T^2(a) - Z_{12}^2 - Z_{22}^2(a)}{2Z_{12}Z_{22}(a)}\right) \tag{12b}$$

where

$$Z_T(s) = Z_{11} + Z_{21} + Z_{12} + Z_{22}(s) \tag{12c}$$

$$Z_T(a) = Z_{11} + Z_{21} + Z_{12} + Z_{22}(a). \tag{12d}$$

Since 100-percent transfer of power occurs when the phase shift between the modes is π, these relations yield N_T, the number of strips for 100-percent transfer, directly as

$$N_T = \frac{\pi}{\phi(a) - \phi(s)}. \tag{13}$$

The preceding derivation is referred to as the full theory. Substantial simplification is possible if the following conditions are met:

a) $K^2 \ll 1$;
b) $\mu = 0$;
c) θ is not in the region of $n\pi$.

Condition a) holds for all known piezoelectric substrates; condition b) will be shown to be acceptable; condition c) means that the simplified expression is not valid in the region of the stopbands. Under these conditions the elapse angles for the passive elements of the line can be equated

$$\phi_1(s) = \phi_1(a). \tag{14a}$$

For the active elements

$$\phi_2(s) = \cos^{-1}\left\{\cos(\theta_2) + \sin(\theta_2) \cdot \left(\frac{2FK^2\gamma}{\theta_2}\sin^2(\theta_2/2)\right)\right\} \tag{14b}$$

$$\phi_2(a) = \cos^{-1}\left\{\cos(\theta_2) + \sin(\theta_2) \cdot \left(\frac{2FK^2(\gamma-1)}{\theta_2}\sin^2(\theta_2/2)\right)\right\}. \tag{14c}$$

Then the difference of the arccosines may be simplified to give

$$N_T = \frac{\pi}{FK^2}\,\frac{\theta/2}{\sin^2(\theta/2)} \tag{15}$$

where

$$\theta = \frac{2\pi f \alpha d}{v}. \tag{16}$$

This expression is similar to the estimate (5) for an anisotropic film of sampled and averaged conductivity as considered in Section II-C.

Throughout this paper a frequency scale normalized to the first structure stopband is used on the assumption that MSC behavior scales with repeat distance. Thus, $f_n = f/f_0 = \theta/\pi\alpha$.

The N_T expression for a perfectly anisotropic film may be obtained from (3) as

$$N_T = \frac{2}{K^2}\left(\frac{f}{f_0}\right)^{-1}. \tag{17}$$

On a plot of N_T against frequency, this gives a rectangular hyperbola. The simplified expression (15) differs in that sampling and averaging effects have become incorporated. The result is a U-shaped curve as demonstrated by the dotted curve of Fig. 4. The full expression (13) further incorporates stopband effects due to structure periodicity.

5) N_T as a Function of Frequency: N_T, the number of strips for 100-percent transfer between tracks, is plotted against normalized frequency in the region below the second structure

TABLE I

		Coupler Number								
		C1	*C2*	*C3*	*C4*	*C5*	*C6*	*C7*	*C8*	*C9*
Repeat distance	d μm	16	20	20	20	20	32	32	32	32
Stopband frequency	f_0 MHz	108	86	86	86	86	54	54	54	54
Track aperture	l mm	4	3	3	3	3	4	4	4	4
Number of strips	N	700	140	140	140	140	700	700	700	700
Metallization ratio	η	0.45	0.45	0.62	0.17	0.5	0.37	0.34	0.67	0.12
Measurement technique		OE	E	E	E	E	O	OE	O	O
Activity factor	α	0.85	0.85	0.85	0.85	0.85	0.75	0.77	0.85	0.80
Effective coupling constant	FK^2	0.042	0.043	0.0425	0.0345	0.043	0.041	0.0395	0.038	0.0275
Mismatch factor	μ	0	0	0	0	0	0	0	0	0
Model factor	γ	0.45	0.45	0.62	0.17	.05	0.37	0.34	0.67	0.12

Note: Measurement techniques: optical, O; electrical, E.

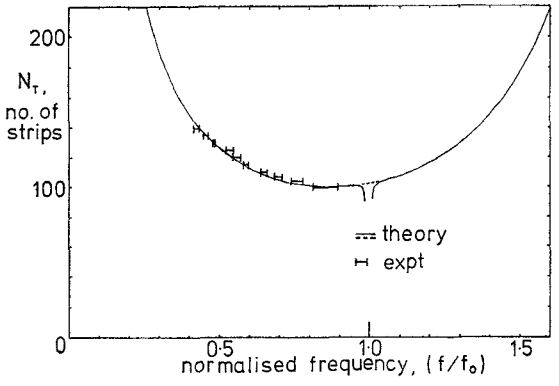

Fig. 4. Number of strips for transfer N_T plotted against frequency normalized to the first stopband frequency, for coupler *C2*.

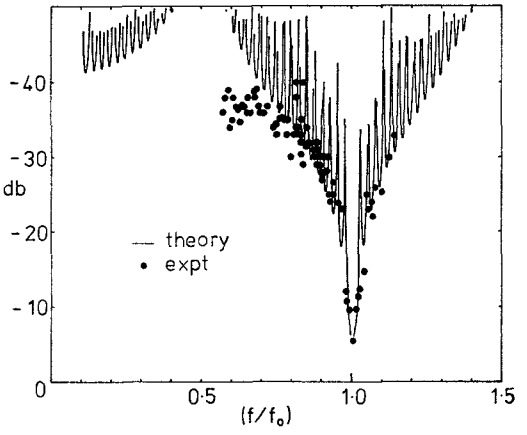

Fig. 5. CW reflection intensity response of MSC *C2*. Theory curve refers to coupler of 40 strips. Experimental points show reflection intensity maxima for coupler of 140 strips.

stopband in Fig. 4. Curve parameters refer to coupler *C2* of Table I as do experimental results shown for comparison. Four specific features may be noted from the curves obtained.

a) There is a clearly defined frequency f_0 at which a stopband occurs.

b) Disregarding the stopband effect (dotted curve), a frequency is obtained at which the number of strips N_T has a minimum.

c) A minimum value of N_T is obtained.

d) The stopband has a characteristic shape.

These features are controlled by separate parameters with relatively little interaction.

a) The stopband frequency comes from the structure repeat distance, $f_0 = v/2d$.

b) The frequency of the minimum for N_T is controlled by the length of the active element of the line αd.

c) The value of the minimum for N_T is determined by FK^2.

d) The shape of the stopband is controlled by the choice of parameters μ and γ.

Comparison between prediction and experiment is deferred to Section IV.

B. Predictions for Transmission and Reflection

1) Transmission: The transmission response for an MSC with a fixed number of strips N is deduced from the value of N_T. For input power P_{in} in track A, output powers are the following:

for track A,

$$P_A = P_{in} \cos^2 (\pi N/2N_T) \tag{18a}$$

for track B,

$$P_B = P_{in} \sin^2 (\pi N/2N_T). \tag{18b}$$

Using the simplified expression (15) for N_T, these may be written

$$P_A = P_{in} \cos^2 (NFK^2 \sin^2 (\pi\alpha f_n/2)/\pi\alpha f_n) \tag{19a}$$

$$P_B = P_{in} \sin^2 (NFK^2 \sin^2 (\pi\alpha f_n/2)/\pi\alpha f_n). \tag{19b}$$

The preceding expressions refer to power transfer for lossless propagation and identical tracks. Experimental and predicted curves are compared in Section IV.

2) Reflection: In the region of the stopband, reflection may be particularly strong because the reflections from individual strips can add constructively. Away from the stopband, though the reflection is weak, its estimation is significant in the design of structures where low triple transit signals are desired.

The reflection is calculated using the two-element model. Steady-state responses for symmetric and antisymmetric modes are calculated independently from the equivalent circuits. A method employing repeated multiplication of section transfer matrices can be used [12]; however, it has been found more convenient to work in terms of an effective characteristic impedance. The computed reflection intensity for the symmetric mode is shown in Fig. 5 for a coupler of 40 strips with the parameters of coupler *C5* (Table I). The frequency response with its 40 zero reflectances below the stopband is typical of the steady-state reflection response of a slightly mismatched lumped line 20 resonant wavelengths long. The computed reflection intensity for the antisymmetric mode is virtually indistinguishable from Fig. 5. The significance of this and of the experimental points shown for a coupler of 140 strips will be discussed in Section IV. The envelope of the reflection response is not affected by the number

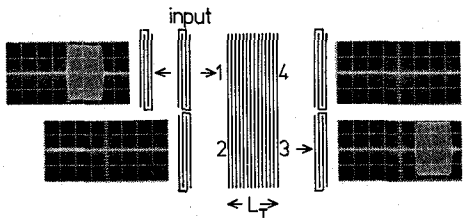

Fig. 6. Transmission and reflection response for a multistrip coupler showing virtually 100-percent transfer.

of strips; for 140 strips, 140 reflection peaks would appear below the stopband.

In pulsed operation, transient reflection responses can be observed associated with reflections from the leading strips; their amplitude is up to 3 dB higher than the CW amplitude. An analysis can be achieved satisfactorily without using the equivalent circuit model; it will not be discussed here.

IV. Prediction Compared with Experiment

A. Experimental Methods

Several experimental methods have been used to investigate the transfer of energy in the coupler. The use of a phase-grating laser probing apparatus has already been described [13]. The apparatus uses first or second diffraction orders of light reflected from the grating formed by a single frequency surface wave [14]. The system is particularly suitable for the examination of multistrip coupler behavior since the surface wave can be probed within the metallized area. Couplers of 700 strips giving many transfers have been examined by this technique. Electrical determinations of the number of strips for transfer have been made. The arrangement of Fig. 1(a) was taken with power input to track A only. Frequencies were noted which gave zero power at just one of the output transducers $A2$, $B2$; this represents the situation of an integral number of transfers. Ambiguity over the number of transfers was removed by referring to optical probing results. Again couplers having 700 strips were examined. In an alternative method couplers of 140 strips were employed to show a single transfer; strips were deactivated by vaporizing the metal at the midpoint of the strips with a laser burner. This yielded a series of single transfer points on the N_T-f_n curve. Full transmission and reflection curves were also obtained at outputs $A2$, $B2$, and $B1$ as a function of frequency for selected couplers.

All measurements reported refer to MSC structures of parallel aluminium strips perpendicular to the Z axis on Y-cut Z-propagating $LiNbO_3$. Parameters for individual couplers are given in Table I. The track aperture quoted refers to the width of individual launching–receiving transducers in each track. The metallization ratio η is defined as the ratio of strip width to repeat distance; a range of metallization ratios was examined with the aims of the following.

1) Obtaining the minimum possible value of N_T.

2) Obtaining the flattest possible curve for N_T against frequency to maximize the bandwidth of the coupler.

3) Obtaining information on the proper circuit model for the full theory.

B. Coupler Performance

The operation of the coupler is demonstrated in Fig. 6. Signal input is at transducer $A1$; the three coupler outputs together with a calibration delay line output are shown in the four photographs. The coupler (device $C2$ of Table I) was of

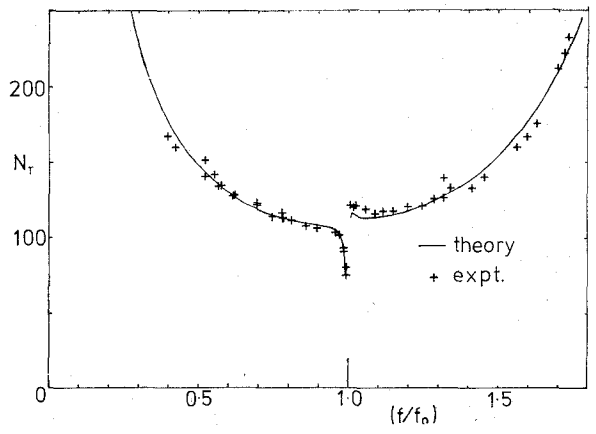

Fig. 7. N_T-f_n curve for coupler $C7$ showing experimental points around and above stopband. A trace of bulk wave interaction at $f_n=1.36$ is visible.

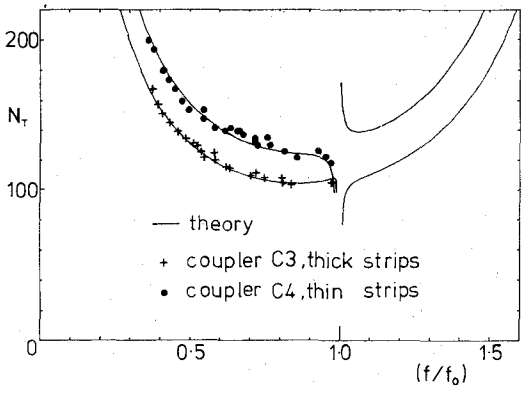

Fig. 8. N_T-f_n curves for metallization ratios 0.62 (coupler $C3$) and 0.17 (coupler $C4$).

140 strips; its stopband frequency was 86 MHz; operation is shown at 43 MHz. The coupler transfer loss was found to be 0.5 dB; the uncoupled surface-wave signal was more than 30 dB down on the coupled signal as was the reflected signal.

C. Experimental Variation of N_T with Frequency Compared with Theory

An example of the result of fitting theory to experimental results is shown in Fig. 4 for coupler $C2$; structure and fitting parameters are listed in Table I. The full curve refers to the full theory; the dotted curve shows the simplified theory where it is distinct from the full curve. Though the full curve is plotted in the stopband region, the electrical method used for obtaining the results does not yield good data there. A better comparison for this region is shown in Fig. 7 for optical results on coupler $C7$.

Above the stopband the fit between theory and experiment is generally more doubtful and the modes are found to be appreciably attenuated in the coupler especially at $f=1.36f_0$. This is attributed to coupling to bulk waves, and some evidence for this has been previously published [13]. We do not consider these interesting effects further here because they are outside the scope of the theory and because from a device point of view their very existence renders this frequency range of little interest.

The results of Fig. 4 are for a coupler of metallization ratio $\eta=0.45$. Results and fitted curves for two couplers of more extreme geometry are shown in Fig. 8. The metallization ratio for thick strips (coupler $C3$) was 0.62 and for thin strips

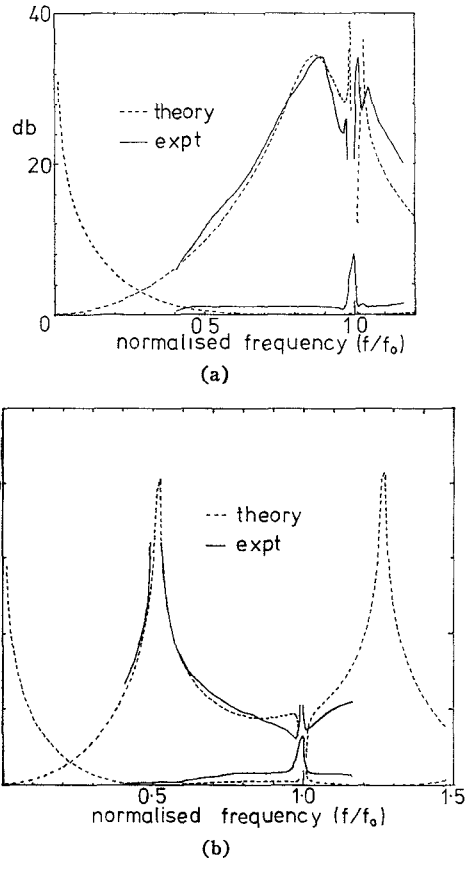

Fig. 9. Experimental and theory curves for energy transmission on two tracks of coupler $C2$. (a) For 100 strips. (b) For 125 strips.

(coupler $C4$) 0.17. Fitting parameters for the curves are given in Table I. Table I also shows results and fitting parameters for further couplers. A curious experimental feature of varying the metallization ratio between its extremes was found to be a reversal of the asymptotic shape of the stopband. The significance of this and other parameter variations is discussed in Section IV-E.

D. Transmission and Reflection Compared with Theory

The transmission response of the basic MSC is shown in Fig. 9; Fig. 9(a) refers to 100 coupler strips and Fig. 9(b) to 125 strips. In both cases the transmitted outputs (in decibels down on the input signal) are plotted against the frequency normalized to the stopband frequency. Full curves refer to experimental results for coupler $C2$ and dashed curves to the full theory. The theory shows a signal null in track A and a stopband; agreement for 100 strips is excellent. The simplified theory gives identical curves outside the stopband region and is adequate for most transmission prediction purposes. Signal loss at maximum transfer for coupler $C2$ at 100 strips was almost 1 dB; however, the normal transfer loss for full length couplers is 0.5 dB.

The reflection response of the MSC is shown in Fig. 5 for the symmetric mode for coupler $C5$ (140 strips). A long pulse is employed to give effectively CW behavior. Experiment gave a closely spaced comb of peaks and troughs as predicted. Only the reflection intensity maxima are plotted, corresponding to the envelope of the theory curve. Agreement in shape and level is quite satisfactory on both sides of the stopband.

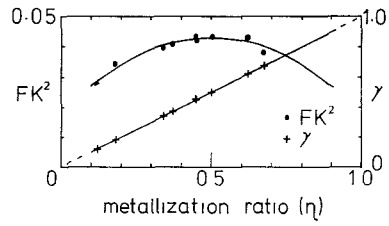

Fig. 10. Variation with surface metallization ratio of effective coupling constant FK^2 and of field model γ. Equation of fitting parabola is $(\eta-0.5)^2=10(0.043-FK^2)$.

Over the MSC working range ($0.6\,f_0$–$0.85\,f_0$), the signal reflected is shown to be more than 30 dB down on the incident signal. Deviation from the theory curve level could possibly be due to mass loading, bulk waves, or coupler imperfections. Methods for further reduction of unwanted reflected signals are discussed in Section VI. Experimental reflection results for the antisymmetric mode for coupler $C3$ gave a similar response shape 3 dB stronger in intensity. Other couplers with $\eta \simeq 0.5$, however, have shown similar intensity levels for the two modes.

E. Discussion of Comparison of Prediction and Experiment

Since in the next section we shall elaborate the equivalent circuit to deal with a wider range of experimental situations, here we will discuss the parameters which have been used to achieve the very satisfactory fit shown between prediction and experiment. Good fits have been obtained with both simplified and full expressions using the fitting parameters F, α, γ, μ for N_T and transmission curves. F and α are common to the two expressions, and common values are employed. They are the crucial parameters from a device viewpoint because they entirely characterize the simplified expression and because they dictate the behavior in the frequency range in which coupler components are constructed (as discussed in [17]). Therefore we consider values of F and α first.

A plot of FK^2 against the metallization ratio η is shown in Fig. 10. The curve drawn is of parabolic form to demonstrate the symmetry about $\eta=0.5$. The result shows a remarkable similarity to the theoretical behavior predicted by previous workers [4], [7] where F is referred to as a geometrical factor. The conclusion is that $\eta=0.5$ gives optimum performance not only in lithium niobate but more generally.

In fitting we have found α, which measures the active length of the section, to show only small inconsistent variation between coupler structures. At first sight this is surprising. In attempting to relate the equivalent circuit of the coupler to the structure of the device one might have anticipated a direct relationship between activity α and metallization η. Our results show that no such direct relationship exists. A similar result has been found by Milsom and Redwood [5] in comparing an exact theory of the transducer on PZT with the equivalent circuit model.

In fitting the full theory we find a direct relation between the field model γ and the metallization ratio η as shown in Fig. 10, though in practice some latitude in γ exists in optimizing the stopband shape. Thus results show that for a structure with ultranarrow strips and wide gaps, an in-line field model is appropriate for the active element while for ultrawide strips and narrow gaps a crossed-field model is appropriate. This easily explains the reversal of asymptotic shape at the stop-

band observed experimentally. Milsom and Redwood have predicted a similar relationship between model and metallization for PZT [5].

There has always been some problem in deciding on the type of equivalent circuit model to adopt for a surface wave, in-line or crossed field. This work strongly suggests that the metallization, in determining the field distribution, also determines the model; the crossed-field model is associated with a high metallization ratio and the in-line model with a low metallization ratio. The idea of an active strip or an active gap now becomes untenable; rather there is a shift of importance from one to the other as metallization increases. Now referring back to the earlier discussion of α, we should no longer anticipate a monotonic relationship between active length and metallization ratio.

The full theory has throughout been fitted with $\mu = 0$. This means that no distinction is made between the velocity in active and passive regions other than through electrical activity. This of course is consistent with the rejection of a fixed identification between strip and gap and active or passive elements. Use of $\mu = 0$ is also attractive in terms of the derivation of the simplified theory. However, it should be stressed that the parameters μ and γ as given in Table I do not constitute a unique set of fitting parameters. The feature of the set presented is that they were obtained with a conscious attempt to make a physical interpretation possible.

V. Extension of Equivalent Circuit Approach

The previous sections have dealt with an MSC which spanned two identical tracks. In this section this restriction is relaxed; results are presented for unequal track widths and the extension of the model to tracks on dissimilar materials is also considered. The equivalent circuit approach is also used to derive an expression for attenuation due to strip resistance and to consider effects of addition capacitive loading such as occurs if the strips span inactive regions between two tracks.

A. Nonidentidal Tracks

1) Unequal Track Widths: The standard MSC has parallel strips on a single substrate; for unequal track widths, since the phase velocities in each track are unchanged, symmetric and antisymmetric modes exist as previously defined. Their velocities are unaffected but the fraction of energy transferable is reduced below 100 percent. Thus the number of strips required for maximum transfer is not affected but the maximum fraction of energy transferred F_T is changed. Analytically F_T is calculated as follows.

From the definition of the symmetric mode, the voltages in each track are equal for every strip. Referring to the equivalent circuit transformer of Fig. 2, the symmetric mode condition is

$$\frac{r_A i_A(s)}{C_A} = \frac{r_B i_B(s)}{C_B}. \tag{20a}$$

From the definition of the antisymmetric mode, the fluxes coupled between tracks must be equal and opposite. Then the antisymmetric mode condition is

$$r_A i_A(a) = r_B i_B(a). \tag{20b}$$

Subscripts A and B refer to the two different tracks, and (s) and (a) refer to the modes. In considering energy transfer, all energy input occurs at track A; the input energy is proportional to current squared, i.e., to $(i_A(s)+i_A(a))^2$. At maximum transfer the energy output at track A is a minimum and is proportional to $(i_A(s)-i_A(a))^2$. Hence the maximum fraction of energy transferred to track B is obtained as

$$F_T = \frac{4 i_A(s) i_A(a)}{(i_A(s) + i_A(a))^2}. \tag{21}$$

Using the preceding mode conditions, the currents may be eliminated to give

$$F_T = \frac{4 C_A C_B}{(C_A + C_B)^2} = \frac{4 l_A l_B}{(l_A + l_B)^2} \tag{22}$$

where l_A and l_B represent track aperture widths. 100-percent transfer is thus only obtained for equal track widths, the case studied previously.

Experimentally the laser probe apparatus has been used to examine the transfer distance as a function of relative track width. As predicted, the transfer distance was found to be unaffected by a change in the relative track widths. Accurate verification of the fraction of power transferred was not possible.

2) Dissimilar Propagation Directions and Dissimilar Materials: Dissimilar propagation directions on the same substrate is a realistic problem to consider because, as discussed in [17], various device applications emerge if the strips in one track are inclined to those in another track. The problems raised are similar to those which exist if the coupler spans two different materials; permittivity, SAW velocity, acoustic impedance, and K^2 are no longer identical. There is no difficulty in incorporating these into the equivalent circuit shown in Fig. 2, associating one set of parameters with line A and the other with line B. However, if the values of K^2 and hence of $\Delta v/v$ differ, it is no longer a simple coupled mode system. It is not possible simultaneously to set up the two modes defined previously (Section III-B). Therefore it is not possible to transform the pair of lines to a single line. Alternative approaches to the problem based on the equivalent circuit model take us beyond the scope of this paper.

B. The MSC with Additional Capacitance

One of the attractions of the equivalent circuit approach to the analysis of the multistrip coupler is the ease with which the effects of electrical loading of the strips can be examined. Capacitative loading is involved in several applications of the coupler. When the coupled acoustic tracks are not directly adjacent, the strips have to be of extra length. Two device examples are the multistrip reflector and the track separator coupler (see [17]). Both rely on velocity mismatching where strips lie on material outside the track apertures to avoid surface-wave generation there. The result of extra length is extra capacitance between strips. Considering equal track apertures l and a track separation Δl, the capacitance increases from C to $(1+\frac{1}{2}\Delta l/l)C$. The consequence is a change in the transformer turns ratio r of Section III which may be incorporated into the calculation as a degradation in the coupling constant K^2. Then

$$K'^2 = (1 + \tfrac{1}{2}\Delta l/l)^{-1} K^2. \tag{23}$$

Thus the number of fingers for transfer is increased by the proportional rise in track capacitance. In the particular example of the multistrip reflector, the number of strips for operation at 50-Ω impedance on *YZ* lithium niobate is predicted to rise from 50 to 60. Experimental results for the 60 finger structure are presented in [17].

C. Strip Resistance and Attenuation

Acoustic attenuation in the MSC can arise from both mechanical and electrical sources, e.g., mode conversion to bulk waves and ohmic loss in the metal strips. It is clear that an appreciable ohmic loss could occur as a result of currents flowing along the length of the strips; this is the particular loss mechanism investigated here. These strip currents flow for the antisymmetric mode but not for the symmetric mode.

For identical tracks the distributed resistance of the strip is replaced by a resistor R_F localized between the acoustic tracks; R_F is set equal to the strip resistance for one track. A finite value of impedance instead of zero impedance is now transformed into the single-line acoustic circuit for the antisymmetric mode [Fig. 3(b)]. This impedance is

$$Z_R = r^2 R_F (1 + 2\pi j f C R_F)^{-1}. \tag{24}$$

Under the condition $2\pi f C R_F \ll 1$ which is easily satisfied, and using the simplified expression (15) for N_T, an amplitude attenuation coefficient α_R per coupler transfer length for the antisymmetric mode is obtained as

$$\alpha_R = 2\pi^2 f C R_F. \tag{25}$$

Resistance per square for the evaporated aluminium films was found to be within 10 percent of the bulk value over a wide range of film thickness and strip dimensions. Thus for a 4-mm-long strip of thickness 5000 Å and width 12 μm, the predicted resistance is 18 Ω ($\rho_{Al} = 2.8 \times 10^{-6} \Omega \cdot$ cm); the measured value was 20 Ω. From transducer measurements a value of order 1 pF per finger was obtained at 54 MHz. Thus for coupler *C7* the predicted value of α_R is 0.02 which represents 0.18 dB per transfer. A measurement for the difference in propagation loss between symmetric and antisymmetric modes, which directly estimates resistive loss, for a coupler of the dimensions of *C7* (Table I) gave a value of 1 dB for seven transfers. Thus prediction and experiment are in good agreement; it is shown that resistive loss in the multistrip structure is quite insignificant.

VI. General Design Criteria for Multistrip Components

Based on the experimental and theoretically predicted behavior of the simpler coupler structure, some general design criteria are now presented which are of relevance both to the coupler itself and to multistrip components derived from it.

A. Substrate

Two important factors follow from the choice of substrate, the space occupied by the MSC and the time necessary to traverse it. Taking the 3-dB coupler as an example (it is the component most extensively used in [17]), the length of an optimized structure is approximately λ/K^2 and the traversal time is $(fK^2)^{-1}$. On *YZ* $LiNbO_3$ this gives a length of about 25 λ and a traversal time at 100 MHz of 0.25 μs. The length is sufficiently small compared to the aperture of a 50-Ω transducer on this material of 108 λ [15] to suggest that the increased surface area occupied is not a significant factor, particularly in structures with delay times exceeding the transit time. On the other hand the MSC is not admissible if the delay time required is less than $(fK^2)^{-1}$. This can be an important factor in rejection of multistrip components at low frequencies or, alternatively, in forcing the operating frequency up if they are to be employed. A further alternative is to raise K^2; this is discussed in [17]. Other materials have a lower K^2 and are therefore less favorable. *ST*-cut quartz, for example, would raise the length to $\sim 10^3$ λ and the traversal time to ~10 μs at 100 MHz. These are unacceptably high for a 3-dB coupler but do not exclude the use of the coupler as a tap on a delay line [17] where significantly fewer strips would be required.

Apart from its high K^2, *YZ* $LiNbO_3$ offers other advantages as a substrate for multistrip components, e.g., zero beam steering, strong self-collimation, and appreciable anisotropy. The latter is an advantage in bent coupler structures where power loss can be avoided on the bends by phase mismatch. Finally, we point out that the broad bandwidth offered by a high K^2 material is entirely compatible with the coupler.

B. Photolithography

Multistrip components require no extra processing stages since the structure can be designed and produced at the same time as the SAW transducers. Optimum MSC performance is obtained for 50-percent metallization so the resolution required photolithographically is similar to that for the interdigital driving transducers; coupler strips are on a slightly smaller scale than the transducer fingers but shorts and breaks are less critical. In operation individual broken or shorted strips can be discounted. The composition and thickness of the metal film do not appear to be significant factors though through mass loading and topographical effects they can affect the degree of bulk mode conversion and reflection from the structure. As illustrated in the previous section, resistive losses in the strips are not significant.

C. Fixing the Frequency of the Stopband and the Number of Strips

Coupler design for a specific application involves choice of the optimum strip repeat distance. The choice is significant when bandwidth is important. Though theory suggests that there are ranges of effective coupling at frequencies above the structure stopband frequency f_0 where $f_0 = v/2d$ (d being the strip repeat distance), experiment has shown that attenuation and spurious signals present severe problems in these ranges The fractional stopband width is found to be of order $1/K^2$; thus $f_0 (1 - 1/K^2)$ can be regarded as the upper frequency limit. The lower limit to the bandwidth range is imposed by the decrease in coupling effectiveness with decreasing frequency. The lower frequency limit for performance is easily defined from the use of the simplified expression for N_T.

Random fingers may be introduced with the aim of eliminating the stopband. Experimentally the problem is to get a wide enough range of strip variation without either significantly increasing photolithographic resolution requirements or vastly extending the coupler length. Small random variations merely widen the stopband rather than remove it. In practice it is reckoned to be better to have a periodic structure

with a narrow stopband and to restrict operation to lower frequencies than to try to spread the stopband.

D. Spurious Signal Reduction

CW and transient reflected signals on $LiNbO_3$ are in general 30 dB down on the input signal. If this level proves significant, a further 10-dB reduction can be obtained by finger length weighting the leading coupler strips to provide a tapered edge; Chebyshev weighing on five fingers has been employed. Practical SAW systems tend to be limited by other spurious signal considerations. Thus it is an attractive feature of the MSC on $LiNbO_3$ that such techniques are not necessary. Employment of the MSC to reduce spurious signal responses in SAW systems is dealt with in [17].

VII. Conclusions

In this paper our objective has been to develop a method of analyzing the behavior of the coupler which leads to useful design criteria. We have shown that in the frequency range where the coupler and its derivatives are used a simple two-parameter expression suffices to predict the behavior. This statement assumes FK^2 is known for the particular material under investigation at 50-percent metallization, a situation which commonly exists from transducer measurements and from theoretical prediction.

The equivalent circuit we have used is very similar to that employed by Milsom and Redwood [5] for transducer structure. A feature of our equivalent circuit-fitting parameters on $LiNbO_3$ which we regard as significant is that they bear a striking similarity to those of Milsom and Redwood on poled PZT. Furthermore, from the predicted behavior of transducer structures on quartz [7], it is apparent that the same trends in parameter would be required. Therefore, we are led to suggest that though differences in detail may exist between the equivalent circuit parameters for couplers on different materials, the parameters found for $LiNbO_3$ have general validity.

Using the equivalent circuit model, inclusion of some important refinements is possible. We have demonstrated the inclusion of finger resistance and additional capacitance and have touched on coupling between dissimilar materials. Furthermore, as discussed in Section IV, the variation of parameters with metallization ratio leads to an interesting identification of model (in-line or crossed field) not with material or its orientation but with the degree of metallization. The cross correlation here between the properties of the multistrip coupler and the interdigital transducer is particularly interesting.

Various aspects of MSC operation have not been fully incorporated into the equivalent circuit. These include mass loading and topographical effects arising from the presence of the metal strips; these would become important at high ratios of film thickness to acoustic wavelength and for low K^2; they can have a major influence on the behavior in the vicinity of the stopband and on the level of reflection from the coupler. The equivalent circuit ignores surface-wave energy conversion to bulk modes which we have observed to be important above the stopband. To deal adequately with all these effects a more sophosticated approach is required such as that of Joshi and White [16] employing the full piezoelectric fluxes and potentials. Such an approach should remove the requirement for the empirical parameters which we introduce into the equivalent circuit.

Acknowledgment

The authors wish to thank J. Oliver for laser probe measurements and A. S. Young for supply of devices; and the Director, Royal Radar Establishment, and the Controller of H. M. Stationery Office for permission to publish this paper.

References

[1] F. G. Marshall and E. G. S. Paige, "Novel acoustic-surface-wave directional coupler with diverse applications," *Electron. Lett.*, vol. 7, pp. 460–462, Aug. 1971.
[2] E. A. Ash and D. P. Morgan, "Realization of microwave circuit functions using acoustic surface waves," *Electron. Lett.*, vol. 3, pp. 462–463, Oct. 1967.
[3] W. L. Bond, J. H. Collins, H. M. Gerard, T. M. Reeder, and H. J. Shaw, "Acoustic surface wave coupling across an air gap," *Appl. Phys. Lett.*, vol. 14, pp. 122–124, Feb. 1969.
[4] S. G. Joshi and R. M. White, "Excitation and detection of surface elastic waves in piezoelectric crystals," *J. Acoust. Soc. Amer.*, vol. 46, pp. 17–27, July 1969.
[5] R. F. Milsom and M. Redwood, "Interdigital piezoelectric Rayleigh wave transducer: An improved equivalent circuit," *Electron. Lett.*, vol. 7, pp. 217–218, May 1971.
[6] J. J. Campbell and W. R. Jones, "A method for estimating optimal crystal cuts and propagation directions for excitation of piezoelectric surface waves," *IEEE Trans. Sonics Ultrason.*, vol. SU-15, pp. 209–217, Oct. 1968.
[7] G. A. Coquin and H. F. Tiersten, "Analysis of the excitation and detection of piezoelectric surface waves in quartz by means of surface electrodes," *J. Acoust. Soc. Amer.*, vol. 41 pp. 921–939, Apr. 1967.
[8] R. F. Milsom and M. Redwood, "Piezoelectric generation of surface waves by interdigital array," *Proc. Inst. Elec. Eng.*, vol. 118, pp. 831–840, July 1971.
[9] W. R. Smith, H. M. Gerard, J. H. Collins, T. M. Reeder, and H. J. Shaw, "Analysis of interdigital surface wave transducers by use of an equivalent circuit model," *IEEE Trans. Microwave Theory Tech.*, vol. MTT-17, pp. 856–864, Nov. 1969.
[10] T. Kraiojananan and M. Redwood, "Equivalent electrical circuits of interdigital transducers for piezoelectric generation and detection of Rayleigh waves," *Proc. Inst. Elec. Eng.*, vol. 118, pp. 305–310, Feb. 1971.
[11] D. A. Berlincourt, D. R. Curran, and H. Jaffe, "Piezoelectric and piezomagnetic materials and their function in transducers," in *Physical Acoustics*, W. P. Mason, Ed., vol. 1A. New York: Academic Press, 1964, pp. 233–242.
[12] E. K. Sittig and G. A. Coquin, "Filters and dispersive delay lines using repetitively mismatched ultrasonic transmission lines," *IEEE Trans. Sonics Ultrason.*, vol. SU-15, pp. 111–119, Apr. 1968.
[13] J. D. Maines, F. G. Marshall, J. F. C. Oliver, and E. G. S. Paige, "Frequency dependent behaviour of an acoustic-surface-wave multistrip coupler," *Electron. Lett.*, vol. 8, pp. 81–82, Feb. 1972.
[14] R. L. Whitman and A. Korpel, "Probing of acoustic surface perturbations by coherent light," *Appl. Opt.*, vol. 8, pp. 1567–1576, Aug. 1969.
[15] W. R. Smith, H. M. Gerard, J. H. Collins, T. M. Reeder, and H. J. Shaw, "Design of surface wave delay lines with interdigital transducers," *IEEE Trans. Microwave Theory Tech.*, vol. MTT-17, pp. 865–873, Nov. 1969.
[16] S. G. Joshi and R. M. White, "Dispersion of surface elastic waves produced by a conducting grating on a piezoelectric crystal," *J. Appl. Phys.*, vol. 39, pp. 5819–5827, Dec. 1968.
[17] F. G. Marshall, C. O. Newton, and E. G. S. Paige, "Surface acoustic wave multistrip components and their applications," this issue, pp. 216–225.